Tailoring chemical and physical properties of fibrous scaffolds from block copolyesters containing ether and thio-ether linkages for skeletal differentiation of human mesenchymal stromal cells

Tailoring Chemical and Physical Properties of Fibrous Scaffolds from Multiblock Copolyesters Containing Ether and Thio-ether Linkages for Skeletal Differentiation of Human Mesenchymal Stromal Cells

Honglin Chen[§], Matteo Gigli[§], Chiara Gualandi, Roman Truckenmüller, Clemens van Blitterswijk, Nadia Lotti, Andrea Munari, Maria Letizia Focarete[*], Lorenzo Moroni[*]

H. Chen,[§] Dr. R. Truckenmuller, Prof. C. van Blitterswijk, Dr. L. Moroni

Department of Complex Tissue Regeneration

MERLN Institute for Technology Inspired Regenerative Medicine

6200 MD Maastricht, The Netherlands

E-mail: l.moroni@maastrichtuniversity.nl

Dr. M. Gigli,[§] Prof. N. Lotti, Prof. A. Munari

Department of Civil, Chemical, Environmental and Materials Engineering

University of Bologna

40127 Bologna, Italy

Dr. C. Gualandi, Prof. M.L. Focarete

Department of Chemistry ‘‘G. Ciamician’’ and INSTM UdR of Bologna

University of Bologna

40126 Bologna, Italy

E-mail: marialetizia.focarete@unibo.it

Prof. M.L. Focarete

Health Sciences and Technologies – Interdepartmental Center for Industrial Research (HST-ICIR), University of Bologna

40064 - Ozzano dell'Emilia (Bologna), Italy

§ equally contributing authors

Keywords: aliphatic copolyesters, ether and thioether linkages, electrospun scaffolds, human mesenchymal stromal cells, skeletal differentiation

Abstract

Scaffold-based tissue engineering holds a promising strategy for repairing damaged tissues and organs. Therefore, there is a great need for new biodegradable polymers, like polyesters, to fabricate bioactive scaffolds in regenerative medicine. In the present study, new functional electrospun scaffolds were successfully fabricated from a class of multiblock poly(butylene succinate)-based (PBS-based) copolyesters containing either butylene thiodiglycolate (BTDG) or butylene diglycolate (BDG) sequences. The polyesters displayed tunable mechanical properties and hydrolysis rate depending on the molecular architecture and on the kind of etheroatom introduced along the polymer backbone. To investigate their potential for skeletal regeneration, human mesenchymal stromal cells (hMSCs) were cultured on the scaffolds in basic, osteogenic and chondrogenic media. Our results demonstrated that PBS-based copolyesters containing thio-ether linkages (i.e. BTDG segments) were more favorable for chondrogenesis of hMSCs than those containing ether linkages (i.e. BDG sequences). In contrast, PBS-based copolyesters containing ether linkages showed enhanced mineralization. These new functional scaffolds hold, therefore, potential for the regeneration of osteochondral tissues by tailoring their chemical composition.

1. Introduction

A promising strategy for repairing damaged tissues and organs is to design scaffolds able to support and eventually control cell activity, i.e. adhesion, proliferation and differentiation. Electrospinning is a simple technique capable of producing non-woven scaffolds made of continuous fibers with diameters ranging from few tens of nanometers up to several micrometers.[1] The resulting fibrillary networks mimic the morphology of native extracellular matrix (ECM), which serves to organize cells and provides signals for cellular responses.[2]

Among the manifold of current commercially available thermoplastic materials used to fabricate 3D scaffolds for regenerative medicine, aliphatic polyesters undoubtedly represent so far the most extensive studied class, since they combine good physico-chemical and mechanical properties with assessed biocompatibility.[3] Poly(lactic acid) (PLA), poly(glycolic acid) (PGA), poly(ε-caprolactone) (PCL) and their copolymers are typically used[4] and their hydrolytic and enzymatic degradation under physiological conditions has been extensively proven.[3]Although these polymers have found many applications in clinical practice, the wide tuning of their mechanical, physico-chemical and biological properties is somehow limited.[4] For instance, the copolymerization of PLA with PCL enables to decrease polymer elastic modulus, thus obtaining more deformable materials that, however, are highly hydrophobic and display a very slow degradation rate. Hydrophilicity and hydrolysis rate can be significantly enhanced through copolymerization of PLA with PGA but, in this case, the rigidity of the material persists. This hampers the fabrication of 3D scaffolds capable of adapting to the needs of the specific tissue to be regenerated. Therefore, new polyesters with more flexibility in tuning their properties attract considerable attention in regenerative medicine.

In the last few years, an increasing number of researchers proposed poly(butylene succinate) (PBS) as a possible alternative to the above mentioned aliphatic polyesters due to the following advantages: (i) simple synthetic strategy through melt polycondensation; (ii) low cost of raw

materials (1,4-butanediol and succinic acid), which can be also obtained from renewable resources;[5] (iii) high melting temperatures among poly(alkylene dicarboxylate)s (T_m=113-115°C); (iv) good thermal stability (thus a wide processing temperature range); (v) proven biodegradability and biocompatibility.[6] Furthermore, PBS is already commercialized by different companies for various applications such as compost bags and mulching films, but also fishery, civil engineering and construction and for common household goods.

Many efforts have been recently devoted to target PBS modification aiming to achieve better performances with respect to the intended application. For biomedical applications, composites have been realized by incorporating organic or inorganic fillers such as chitosan, collagen, calcium phosphate or hydroxyapatite along the PBS macromolecular chain.[6] A plethora of PBS-based blends and copolymers have been also obtained.[6] Among other copolymerization techniques, reactive bending is a versatile and solvent free approach which permits to prepare multiblock copolymers of different molecular architecture by simply varying the reaction time.[7]

Recent studies have demonstrated that the properties of scaffold, such as scaffold elasticity, structure and organization, and chemistry, can direct stem cell differentiation into specific lineage.[8] In this study, electrospun scaffolds fabricated from a class of multiblock PBS-based copolyesters containing either butylene thiodiglycolate (BTDG) or butylene diglycolate (BDG) sequences, obtained by reactive blending, are presented. In particular, the possibility to use the synthesized copolymers as an alternative to conventional polyesters was explored to achieve enhanced control over stem cell differentiation. In these systems, the addition of heteroatoms along the macromolecular chains has been demonstrated to tune chain flexibility, thus affecting polymer crystallinity and mechanical properties of aliphatic polyesters.[9, 10] Moreover, through this strategy surface hydrophilicity has been modified, due to the presence of electronegative oxygen and sulphur atoms.[11] All these factors significantly impact the biodegradation rate and biocompatibility of the final materials.[12] Scaffolds with tailored chemical composition and physical properties have been prepared and characterized. Their hydrolytic degradation profile has been evaluated under

physiological conditions. Finally, we show that these copolymers may have the potential to steer human mesenchymal stromal cells (hMSCs) differentiation towards skeletal lineages.

2. Results and discussion

2.1. Electrospinning and sample characterization

PBS, poly(butylene diglycolate) (PBDG) and poly (butylene thiodiglycolate) (PBTDG) displayed a similar chemical structure, all containing two ester groups per repeating unit along a saturated aliphatic chain (**Figure 1)**. With respect to PBS, differences can be observed in the acid sub-units: PBDG contains an ether bond while PBTDG a thioether bond. We previously demonstrated that these minimal differences in the polymer backbone have a remarkable effect on polymer thermo-mechanical properties.[9, 10] In the present study, physical blends of PBS with PBDG and PBTDG and copolymers of PBS containing either BDG or BTDG units with long block length were considered for scaffold fabrication, since these polymeric systems possess physico-chemical and mechanical characteristics significantly different from each other and from the PBS homopolymer. The molecular characterization of the polymeric systems investigated in the present work is reported in **Table 1**.

Electrospinning conditions parameters were optimized in order to obtain defect-free fibres. The scaffolds were highly porous with microscale interstitial pores made of randomly oriented fibres. In the case of Poly(butylene succinate/diglycolate) copolyester ($P(BS_{11}BDG_{11})$), two different polymeric solutions were prepared to obtain scaffolds with either micrometric or nanometric diameters (i.e. 890 ± 410 nm and 410 ± 160 nm) that were labelled $P(BS_{11}BDG_{11})$-m and $P(BS_{11}BDG_{11})$-n, respectively (Figure 1 and **Table S1)**.

Electrospun fibres were characterized by thermogravimetric analysis (TGA) and differential scanning calorimetry (DSC). TGA did not reveal residual solvents in the fabricated fibres and confirmed that electrospinning process did not affect polymer thermal degradation behaviour. DSC was used to evaluate thermal transitions in the electrospun mats (Table 1). The calorimetric data of

$P(BS_{11}BDG_{11})$-m and $P(BS_{11}BDG_{11})$-n were identical within the experimental errors. The phase behaviour of the polymers under investigation was similar. As far as the glass transition phenomenon is concerned, only one glass transition temperature (T_g) was always clearly evident suggesting the presence of a homogeneous amorphous state. All polymers were semicrystalline, being the corresponding calorimetric traces (**Figure S1**) characterized by a significant melting endotherm. The overall heat of fusion (ΔH_m) decreased from blends to block copolymers because of the reduced length of crystallisable sequences. The copolymer containing ether-oxygen showed a slightly bigger ΔH_m associated to the PBS crystal phase compared to the thioether containing copolymer. This implied that the PBS crystallization was less hampered in the copolymer containing BDG co-units. Interestingly, in the PBS/PBDG blend two distinct melting phenomena were evident, suggesting the simultaneous presence of the crystalline phases of the two homopolymers. This result has been previously confirmed by X-ray analyses.[10] For the blends, the melting temperature (T_m) was equal to that of PBS (and of PBDG homopolymer in the case of PBS/PBDG), while it decreased in the multiblock copolymers because of the formation of a less perfect crystalline phase.

In order to investigate the effect of polymer chemistry on material hydrophilicity, water contact angle (WCA) measurements were performed on hot-pressed films and the results reported in Table 1. The significant decrease of WCA values in blends and copolymers was due to the introduction of highly electronegative atoms (O and S) along the PBS polymeric chain, which has the effect of increasing material surface wettability, as previously reported for other polymeric systems.[11, 12, 13] The polymers containing BDG repeating units displayed a lower WCA than those containing BTDG units. Thus, the former were more hydrophilic as a consequence of the higher electronegativity of oxygen atoms with respect to sulphur ones.

In order to correlate bulk mechanical properties with polymer chemical structure, tensile stress-strain measurements were carried out on polymeric films rather than electrospun fibers. Indeed, it is somewhat difficult to make a direct comparison among stress-strain data of non-woven electrospun

fibrous matrices since it is already established that mechanical data depend not only on the type of polymeric material and on single fiber features, but also on the arrangement of the fibers in the nonwoven matrices, such as fiber direction in the mat, fiber curvature, fiber interconnections, fiber fusion at contact points and mat porosity.[14] Elastic modulus (E), stress at break (σ_b) and elongation at break (ε_b) of PBS, PBS/PBTDG, poly(butylene succinate/thiodiglycolate) copolyester (P($BS_{10}BTDG_{10}$)), PBS/PBDG, and P($BS_{11}BDG_{11}$) are reported in **Figure 2**. Both the two blends and the copolymers were characterized by a lower elastic modulus than PBS and by a higher elongation at break (with the only exception of PBS/PBDG). Moreover, E and ε_b were respectively lower and higher in the case of block copolymers compared to the corresponding blends. This behaviour could be due to the decrease in the amount of hard crystal phase when comparing the blend with the corresponding copolymer (Table 1). The presence of thioether bonds along the polymer backbone caused an increase of the elongation at break and a decrease of the elastic modulus compared to the polymers containing ether linkages with the same molecular architecture. This result could be ascribed to the higher chain flexibility of BTDG units due to the presence along the polymeric chain of C-S bonds longer than the C-O ones and due to weaker interchain interactions because of the lower electronegativity of sulphur atoms compared to oxygen ones.

2.2. Hydrolytic degradation

Hydrolytic degradation experiments were performed under physiological conditions on the electrospun mats in order to evaluate the effect of the following factors on the hydrolysis rate: (i) introduction of hydrophilic BDG and BTDG co-units in the PBS macromolecular chain; (ii) type of etheroatom (O or S) introduced; (iii) different molecular architecture (blend or multiblock copolymer). Hydrolytic degradation of these scaffolds can be interpreted on the basis of two different factors: crystallinity degree and surface hydrophilicity. [15]

Comparable results were obtained for both P($BS_{11}BDG_{11}$)-m and P($BS_{11}BDG_{11}$)-n indicating that the fiber diameters considered in the present work did not affect degradation rate. Therefore, for this polymer, average results of the two mats were reported (**Figure 3**). After 162 days of incubation,

PBS practically did not lose weight whereas polymer blends and block copolymers appreciably degraded. In particular, ether-oxygen containing polyesters showed a higher degradation rate with respect to sulphur containing ones. Moreover, Figure 3A shows that the weight loss of block copolymer is higher than the corresponding blend. The trend was particularly evident if we consider PBS/PBDG and P($BS_{11}BDG_{11}$). On the contrary, only a small difference has been recorded in the case of PBS/PBTDG and P($BS_{10}BTDG_{10}$).

Overall, copolymers containing BDG sequences degraded faster than those containing BTDG ones because of the higher hydrophilicity of the former (Table 1). By comparing the blend with the corresponding copolymer, P($BS_{11}BDG_{11}$) degraded to a higher extent than PBS/PBDG because of the lower crystallinity degree, while the two sulphur containing polymers underwent a similar degradation profile because of their comparable crystallinity degree and hydrophilicity (Table 1). The percentage of residual number average molecular weight for PBS, P($BS_{11}BDG_{11}$) and P($BS_{10}BTDG_{10}$) (M_n res%) is reported in Figure 3B as a function of incubation time. The three samples underwent a decrease of M_n with time, although PBS did not show any weight loss in the time range investigated (Figure 3A). This is not surprising, taking into account that in the first stages of hydrolytic degradation a substantial decrease in molecular weight occurs even if weight losses are still negligible.[16] PBS decrease of M_n was lower due to its high crystallinity degree, high crystal perfection and hydrophobicity, while in the case of copolymers the change of molecular weight was more evident and seemed to be affected by the type of polymer investigated: for P($BS_{11}BDG_{11}$) the M_n decrease was higher than that of P($BS_{10}BTDG_{10}$). The calculation of M_n was not possible for the two blends, because the gel permeation chromatography (GPC) traces of the analysed polymers revealed a shoulder since the very beginning of the incubation period that turned into two partially overlapped peaks. With increasing of the incubation time, a second peak was detectable (Figure 3E). Therefore, to monitor the degradation process, the molecular weight of both peaks ($M_{p,}1$ and $M_{p,}2$) was calculated (**Table S2**). For both blends the position of one peak slightly changed (M_p,2), while M_p,1 remarkably decreased with the increase of incubation time. By

considering the difference in repeating units hydrophilicity, we can reasonably assume that M_p,1 is related to either PBDG or PBTDG macromolecular chains that underwent a substantial hydrolytic degradation, while M_p,2 corresponds to PBS macromolecular chains, whose molecular weight decrease was significantly lower.

In order to gain a better understanding of the hydrolysis mechanism occurring in the polymers, ^{1}H-NMR measurements were performed on degraded retrieved samples. Figure 3C reports the content of BS units in mol%, at a certain time of degradation, normalized to the initial mol% BS (mol%BS_t/mol%BS_0) as a function of degradation time. In all samples, an evident increase of BS content and a consequent decrease in the BDG and BTDG content was observed during degradation. The polymeric systems containing ether linkages (PBS/PBDG and P($BS_{11}BDG_{11}$)) underwent a significant change of molar composition, more evident in the blend compared to the copolymer. On the other hand, PBS/PBTDG and P($BS_{10}BTDG_{10}$), underwent a similar decrease of BTDG content. By comparing weight loss (Figure 3A) and chemical composition of the retrieved samples (Figure 3C), it is evident that samples undergoing higher weight loss concomitantly displayed a higher increase of BS units. Therefore, the weight loss was mainly due to the solubilisation of either BDG or BTDG chain fragments since ester cleavage preferentially occurred on etheroatom-containing chain segments, which were easily solubilized in water due to their hydrophilic nature. Moreover, as expected, ether-oxygen-containing sequences demonstrated higher solubility in water with respect to sulphur-containing ones: the lower decrease in molecular weight and the contemporary higher weight loss of P($BS_{11}BDG_{11}$) with respect to P($BS_{10}BTDG_{10}$), indicated that longer BDG sequences were solubilized in water generating a more pronounced change in BS mol%.

A confirmation that the amorphous regions of a polymer degraded more quickly than the crystalline ones was obtained by analysing the degraded samples with DSC. All the calorimetric traces were found to be characterized by an endothermic peak associated with the fusion process of the crystalline portion of the material (similar to Figure S1). The corresponding heat of fusion, at a certain time of degradation, was normalized to the heat of fusion of the corresponding non-degraded

sample ($\Delta H_t/\Delta H_0$). In all the polymeric compositions, the normalized heat of fusion regularly increased with incubation time, with the exception of PBS, whose crystallinity degree was not significantly affected (Figure 3D). It is worth remembering that the increment of the crystalline/amorphous ratio can be also due to annealing, which occurs at a temperature comprised between T_g and T_m (i.e. 37 °C in our case). The increase of $\Delta H_t/\Delta H_0$ can, therefore, be considered as the sum of two contributions: (i) the higher degradation of the amorphous region with respect to crystalline one and (ii) annealing. In block copolymers, the annealing process plays a greater role than in the blends because of the lower crystallization rate of the former, as previously reported.[10,11] As a matter of fact, the crystallization process becomes more difficult as the BS block became shorter due to the effect of the second block (either BDG or BTDG), which limited the transport of the BS blocks on the crystal surface and acted as defect during chain folding. In this respect, the more pronounced increase in the heat of fusion of P($BS_{10}BTDG_{10}$) compared to PBS/PBTDG is not surprising, although they showed a comparable weight loss (Figure 3A). From a comparison between ether-oxygen-containing polymers and sulphur-containing ones, the higher increase in the heat of fusion of the former can be explained on the basis of their higher degradation rate.

2.3. Investigation of hMSCs on scaffolds

To examine the performance of these new polyesters for skeletal tissue engineering, hMSCs were cultured on the samples for 28 days in basic medium (BM), osteogenic medium (OM), chondrogenic medium (CM), or mineralization medium (MM). BM is a maintenance medium that does not trigger the osteogenic and chondrogenic differentiation of hMSCs, while CM is able to support the chondrogenic differentiation of hMSCs.[17, 18] OM is a medium that supports the osteogenic differentiation of hMSCs and MM is a medium that also promotes the formation of a mineralized matrix.[18, 19] The bioactivity of hMSCs was assessed by monitoring the Glycosaminoglycans (GAG) production, cellular morphology, cellular metabolism, alkaline phosphatase (ALP) activity, and relative osteogenic and chondrogenic gene expressions. Polystyrene tissue culture plates were used as a positive control (data not shown). To investigate for

a possible influence of fiber diameter, scaffolds of the same chemistry but different fiber diameter were assessed between P($BS_{11}BDG_{11}$)-n (430 ± 260 nm) and P($BS_{11}BDG_{11}$)-m (890 ± 410 nm). To investigate the effect of the introduction of a co-monomer (either BDG or BTDG) in the PBS chain, scaffolds of similar fiber dimension but different chemical group were examined among PBS, P($BS_{10}BTDG_{10}$) and P($BS_{11}BDG_{11}$)-n. To investigate the effect of reactive blending, PBS/PBTDG and PBS/PBDG scaffolds were considered. Finally, to investigate the effect of blending versus copolymerization, PBS/PBDG blend and P($BS_{11}BDG_{11}$)-m, which had a comparable fiber dimension, were considered.

2.3.1 hMSCs morphology and metabolic activity

Cell attachment and morphology on scaffolds were examined by SEM (**Figure S2**, **Figure S3** and **Figure S4**). After 28 days culture, it could be seen that the hMSCs migrated, attached and proliferated on all types of scaffolds in all investigated media. No significant difference in cell morphology was observed between P($BS_{11}BDG_{11}$)-n and P($BS_{11}BDG_{11}$)-m in all media, indicating that the fiber dimension considered in the present work did not affect cell morphology. In OM, hMSCs on PBS/PBTDG and P($BS_{10}BTDG_{10}$) had a more spread morphology compared to PBS/PBDG and P($BS_{11}BDG_{11}$)-n respectively, therefore revealing an effect of BTDG or BDG presence on cell morphology. However, in CM, hMSCs displayed a morphology with more bi-polar or multipolar extensions on PBS/PBTDG scaffolds in comparison with PBS/PBDG. In addition, no difference in cell morphology was observed between PBS/PBDG blend and its corresponding block copolymer of P($BS_{11}BDG_{11}$) in all media.

Cell metabolic activity on seeded scaffolds was evaluated at days 7 and 28 using a Presto Blue assay (**Figure S5**). Metabolic activity increased over the cell culture period in all media for all scaffolds. P($BS_{11}BDG_{11}$)-n and P($BS_{11}BDG_{11}$)-m had a similar metabolic activity cultured in both BM and CM through the culture time points. In OM, P($BS_{11}BDG_{11}$)-n showed a significantly higher metabolic activity at day 28 compared with P($BS_{11}BDG_{11}$)-m due to their difference in fiber dimension. PBS constructs displayed a slightly higher metabolic activity compared to

P($BS_{10}BTDG_{10}$) in both BM and CM at day 28 due to the presence of co-units of BTDG. Similarly, the presence of BDG blocks along polymer chain did not enhance the cell metabolism in comparison with PBS under the same conditions. Interestingly, in the copolymers the introduction of BDG blocks generated a higher cell metabolism in CM compared to BTDG blocks, while in OM PBS/PBDG displayed higher cell metabolic activity compared to PBS/PBTDG.

2.3.2. ALP activity

To investigate early osteogenic differentiation of hMSCs cultured onto different scaffolds either in BM or in OM , we performed quantitative analysis of ALP at days 7 and 28 (**Figure 4**A and 4B). ALP is commonly known as an early marker of osteogenic differentiation, which is involved in the formation of calcium phosphate crystals.[20] The ALP activity increased during cell culture period in BM and OM and showed no remarkable difference between scaffolds at day 7. After 28 days, P($BS_{11}BDG_{11}$)-m showed a similar ALP activity as P($BS_{11}BDG_{11}$)-n in OM. Shih et al. grew human hMSCs on electrospun type I collagen nanofibers.[21] They demonstrated that no significant difference of ALP activity of hMSCs after 12 days of culture in OM was observed between scaffolds with fiber diameter of 200-500 nm and fiber diameter of 500-1,000 nm. PBS, P($BS_{10}BTDG_{10}$) and P($BS_{11}BDG_{11}$)-n scaffolds supported a similar ALP activity in both BM and OM, which indicated that the presence of block units of BTDG and BDG do not elicit a specific effect on ALP activity. We also observed that ALP activity in both BM and OM was comparable for both PBS/PBTDG and PBS/PBDG. This suggested that the introduction of a second component of the blend, being either PBTDG or PBDG, has a similar effect on ALP activity. It is worth mentioning that the ALP activity on P($BS_{11}BDG_{11}$)-m was higher than the corresponding blend in both investigated media.

The results of ALP activity were further confirmed by staining cells with ALP (**Figure S6** and **S7**). Low levels of ALP staining were present on all types of scaffolds at day 7 in both media without significant difference. P($BS_{11}BDG_{11}$)-n showed similar density in ALP staining during the cell culture period in all media compared to P($BS_{11}BDG_{11}$)-m. At day 28, the intensity of ALP

staining remarkably increased on PBS and P($BS_{10}BTDG_{10}$) scaffolds in BM compared to P($BS_{11}BDG_{11}$)-n, suggesting a possible inductive effect on stem cell early osteogenic differentiation of these two chemical compositions. Furthermore, ALP staining increased in intensity on PBS, P($BS_{10}TDG_{10}$), and P($BS_{11}BDG_{11}$)-n scaffolds in OM. Interestingly, PBS/PBDG and PBS/PBTDG scaffolds exhibited a constantly lower ALP activity at both time point in all media. In addition, P($BS_{11}BDG_{11}$)-m showed a higher ALP staining in OM than the corresponding blend.

2.3.3. GAG assay

The quantification of GAG synthesis is shown in Figure 4C and 4D. No significant differences were found between P($BS_{11}BDG_{11}$)-m and P($BS_{11}BDG_{11}$)-n in BM. However, after 28 days, P($BS_{11}BDG_{11}$)-m had a significant higher GAG deposition than P($BS_{11}BDG_{11}$)-n in CM, due to their difference in fiber dimension. This results is consistent with the findings by Bean et al.[22], who demonstrated that seeding hMSCs onto microfibers at a higher cell density promotes GAG production better than nanofibers. In CM, at day 28, P($BS_{10}BTDG_{10}$) scaffold presented a significant increase in GAG production compared to PBS and P($BS_{11}BDG_{11}$)-n. In addition, PBS/PBTDG displayed a significantly higher GAG amount than PBS/PBDG in CM. Both these results may indicate that the systems containing BTDG units may have a better effect on production of GAG in CM with respect to those containing BDG units. This result could be due to the presence of sulphur atoms along the polymer chain which are always observed in all of GAG.[23] P($BS_{11}BDG_{11}$)-m highlighted a lower GAG production than the corresponding blend in all media, which is in contrast to ALP activity.

2.3.4. The mineralization of hMSCs

Alizarin red staining (ARS) has been used to examine the level of calcium deposition after 28 days (**Figure 5**). There were no apparently differences in ARS between scaffolds in BM. The intensity of ARS onto P($BS_{11}BDG_{11}$)-n scaffolds was higher than both P($BS_{10}BTDG_{10}$) and PBS scaffolds and no significant differences were found between P($BS_{10}BTDG_{10}$) and PBS in MM. These results suggested that the introduction of BDG blocks supported better mineralization when compared to

the introduction of BTDG blocks. No appreciable differences in ARS were observed between PBS/PBTDG and PBS/PBDG, as well as between PBS/PBDG and P($BS_{11}BDG_{11}$)-m for all media.

2.3.5. Osteogenic gene expression

The investigation of osteoblast-related gene expression for hMSCs on scaffolds was performed at day 7 and day 28 (**Figure 6**). In both media investigated, P($BS_{11}BDG_{11}$)-n and P($BS_{11}BDG_{11}$)-m showed a similar osteogenic gene expression including ALP, Runt-related transcription factor 2(RUNX2), Collagen type I alpha 1 (COL1A1) and Bone sialoprotein (BSP), thus confirming that the difference in fiber dimension in the present work did not affect osteogenic differentiation. ALP expression for PBS, P($BS_{10}TDG_{10}$) and P($BS_{11}BDG_{11}$)-n scaffolds were almost the same in BM. However, ALP expression on PBS was higher than on P($BS_{11}BDG_{11}$)-n scaffolds at day 28 in OM. RUNX2 strongly affects hMSCs osteogenic differentiation in the early stage, resulting in enhanced ALP, osteocalcin (OCN), osteopontin (OPN), and BSP expression.[25] The expression of RUNX2 on PBS was higher than that on P($BS_{11}BDG_{11}$)-n scaffolds at both time points in BM. P($BS_{10}BTDG_{10}$) displayed a significant higher expression of RUNX2 at day 7 in BM in comparison with P($BS_{11}BDG_{11}$)-n. COL1A1 is associated with the formation of the ECM, being considered essential for the development of an osteoblastic phenotype.[26] PBS showed a significant higher COL1A1 expression than P($BS_{11}BDG_{11}$)-n after 28 days in BM, although no significant differences were found in OM. BSP, a late marker of hMSCs osteogenic differentiation, is a highly sulphated and glycosylated phosphoprotein in bone matrix.[27] BSP expression on PBS was significantly higher than that on P($BS_{11}BDG_{11}$)-n at day 28 in OM. All gene expression tested did not highlight significant differences between PBS/PBDG and P($BS_{11}BDG_{11}$)-m. These results suggest that PBS scaffolds may elicit a higher early osteogenic differentiation than copolymers containing BDG or BTDG units.

2.3.6. Chondrogenic gene expression

To know the potential of chondrogenic differentiation of hMSCs on the scaffolds under investigation, we evaluated a panel of chondrocyte-related genes: collagen, type II alpha 1

(COL2A1), SOX-9, aggrecan (ACAN) and activated leukocyte cell adhesion molecule ALCAM (**Figure 7**). No significant difference in expression of the investigated gene profiles was observed between P($BS_{11}BDG_{11}$)-n and P($BS_{11}BDG_{11}$)-m despite of their difference in fiber dimension. COL2A1 is a specific marker of hyaline cartilage ECM.[28] P($BS_{11}BDG_{11}$) and P($BS_{10}BTDG_{10}$) scaffolds displayed a higher expression of COL2A1 than PBS scaffolds at day 28 in BM. It could be inferred that the introduction of BTDG and BDG blocks along the PBS macromolecular chain was favourable for COL2A1 expression. The expression of COL2A1 on PBS/PBTDG scaffold was consistently higher than that on PBS/PBDG scaffolds, indicating that the blend containing BTDG units better supported COL2A1 expression compared to BDG units. SOX9, an early marker for chondrogenesis, is the transcriptional activator of COL2A1, COL9A1 and ACAN.[29] The expression of SOX9 was similar for all scaffolds at both time points in BM, while the expression of this gene significantly increased onto PBS/PBTDG scaffold at day 28 in CM. ALCAM is expressed on human articular chondrocytes and function as a marker for stemness.[30] At day 28, PBS/PBTDG scaffolds supported a significant higher expression of ALCAM in both BM and CM compared to PBS/PBDG scaffolds, thus suggesting that the blend containing BTDG units better supports ALCAM expression compared to BDG units. ACAN is one of the main proteoglycan in the articular cartilage matrix.[31] In BM, ACAN on P($BS_{10}TDG_{10}$) scaffold showed a significant up-regulation compared to PBS, due to the presence of BTDG units along the polymer chain. A significant higher expression of ACAN was observed on PBS/PBTDG scaffold compared to that on PBS/PBDG in both condition media at day 28. Together, gene expressions results indicated that BTDG units displayed better support of hMSCs chondrogenesis with respect to BDG units. This result could be ascribed to the presence of sulphur atoms in the BTDG units. It is also worth noticing that PBS/PBTDG blends showed better performances than the corresponding block copolymer.

3. Conclusions

In the present study, PBS-based scaffolds from multiblock copolymers containing etheroatoms have been successfully prepared by electrospinning. Hydrolytic degradation studies under physiological conditions showed that the hydrolysis rate can be tuned by acting on the kind of etheroatom introduced and on the molecular architecture, as these factors deeply influence both the crystallinity and the surface wettability of the investigated materials**.** The presence of BTDG units in the copolymers demonstrated a better support of chondrogenic differentiation of hMSCs compared to the presence of BDG units. Additionally, PBS scaffolds induced enhanced early osteogenic differentiation of hMSCs and the additional presence of ether units (BDG) resulted in enhanced mineralization. It was also worth mentioning that the same chemical composition, but a different molecular architecture (i.e. blend or multiblock copolymer) highlighted a very different effect on hMSCs cell function such as differentiation. Therefore, molecular architecture revealed as an important parameter in terms of modulating the chemistry of scaffold. These results demonstrated that the new copolymer family may therefore find applications for the regeneration of skeletal tissues in regenerative medicine by tuning their physicochemical properties.

4. Experimental Section

Materials: Dimethylsuccinate (DMS), 1,4-butanediol (BD), diglycolic acid (DGA), thiodiglycolic acid (TDGA), and titanium tetrabutoxide (TBT) (Sigma-Aldrich, Milan, Italy) were reagent grade products. All the reagents were used as supplied with the exception of TBT which was distilled before use. Chloroform, dichloromethane (DCM), 2-chloroethanol (CE) and hexafluoro-2-propanol (HFIP) were purchased from Sigma-Aldrich and were used without any further purification.

Polymer synthesis: Starting homopolymers - i.e. PBS, PBDG and PBTDG - were synthesized in bulk by the usual two steps melt polycondensation, starting from 1,4-butanediol (BD) and DMS, DGA or TDGA, as reported elsewhere.[9, 10] Two blends, PBS/PBDG and PBS/PBTDG, were obtained by melt mixing for 10 min equimolar amounts of PBS with PBDG and PBTDG, respectively, according to the procedures previously described.[9, 10] P($BS_{11}BDG_{11}$) and P($BS_{10}BTDG_{10}$) copolymers were obtained by melt mixing equimolar amounts of PBS with either

PBDG (for 30 min) or PBTDG (for 45 min), respectively. The reactive blending provided two multiblock copolymers (P($BS_{11}BDG_{11}$) and P($BS_{10}BTDG_{10}$)) with similar block length.

Scaffold and film preparation: PBS, PBS/PBDG and PBS/PBTDG blends and P($BS_{11}BDG_{11}$) and P($BS_{10}BTDG_{10}$) copolymers were subjected to electrospinning to obtain 3D mats. Scaffolds were produced by using a customized electrospinning apparatus, comprised of a high-voltage power supply (SL 50 P 10/CE/230; Spellman), a syringe pump (KD Scientific 200 series), a glass syringe, a stainless steel blunt-ended needle (inner diameter = 0.84 mm) connected with the power supply electrode, and a grounded aluminium plate-type collector (7 cm × 7 cm). Polymer solution was dispensed through a Teflon tube to the needle which was placed vertically on the collecting plate at a measured distance (D). The scaffolds were produced at RT and a relative humidity of 40 ± 5%. The electrospun solution and the operating conditions for each polymer were selected after optimization experiments aimed at obtaining bead-free fibers and are reported in Table S1. Electrospun mats were kept under vacuum over P_2O_5 at RT overnight to remove residual solvents.
Films (0.2 mm thick) of PBS, blends and copolymers were obtained by compression moulding the polymers between Teflon plates, with an appropriate spacer, at 140 °C for 1 min under a pressure of 2 ton m^{-2} (Carver C12, laboratory press).

Material characterization: Polymer structure and composition were determined by means of proton nuclear magnetic resonance (^{1}H-NMR) spectroscopy at RT, employing a Varian Inova 400-MHz instrument (Agilent Technologies, USA). Molecular weights were evaluated by gel-permeation chromatography (GPC) at 30°C using a 1100 HPLC system (Agilent Technologies, USA) equipped with PLgel 5-μm MiniMIX-C column (Agilent Technologies, USA). A refractive index was employed as detector. Chloroform was used as eluent with a 0.3 mL/min flow and sample concentrations of about 2 mg/mL. A molecular weight calibration curve was obtained with polystyrene standards in the range of molecular weight 2000-100,000 g/mol. TGA was carried out under nitrogen atmosphere using a Perkin Elmer TGA7 apparatus (gas flow: 30 mL/min) at 10 °C/min heating rate, up to 900 °C. Calorimetric measurements were conducted by using a Perkin

Elmer DSC7 instrument. In the typical setup, the external block temperature control was set at -120 °C and weighed samples of c.a. 10 mg were heated up to 40 °C above fusion temperature at a rate of 20 °C/min. SEM observations were carried out using a Philips 515 SEM (FEI, Eindhoven, The Netherlands) at an accelerating voltage of 15 kV, on samples sputter coated with gold. The distribution of fibre diameters was determined through the measurement of approximately 150 fibres by means of an acquisition and image analysis software (EDAX Genesis, New York, USA), and the results were given as the average diameter ± standard deviation. Static contact angle measurements were performed on polymer films using a KSV CAM101 (KSV, Espoo, Finland) instrument at ambient conditions, by recording the side profiles of deionized water drops for image analysis. Five drops were observed on different areas for each film, and contact angles were reported as the average value ± standard deviation. Stress-strain measurements were performed with an Instron 4465 tensile testing machine equipped with a 100N load cell on rectangular films, according to ASTM D882-02 standard. Sample were 5 mm wide, the gauge length was 20 mm and the cross-head speed was 5 mm/min. Load-displacement curves were obtained and converted to stress-strain curves. At least six replicate specimens were run for each sample and results were provided as the average value ± standard deviation.

Hydrolytic degradation studies: Hydrolytic degradation studies were carried out on rectangular mats of PBS, blends and copolymers in triplicate. Prior to degradation experiments, each specimen was dried over P_2O_5 under vacuum at RT, and weighed to obtain the sample initial mass. Mats were individually immersed in phosphate buffered solution (0.1 M, pH = 7.4) and incubated in a SW22 Julabo shaking water bath at 37 °C and 50 rpm. The buffer solution was periodically changed to keep the pH constant during the entire time scale of the degradation experiments. At different time intervals, triplicate specimens for each sample were recovered from the bath, repeatedly washed with deionized water and dried over P_2O_5 under vacuum to constant weight. The mass loss was determined gravimetrically by comparing the dry weight remaining at a specific time with the initial sample weight. The molecular weight of each recovered sample was determined by GPC. ^{1}H-NMR

analysis was performed to detect changes in the molecular composition during the hydrolysis experiments and DSC was used to evaluate the change in crystallinity degree.

Cell culture and seeding: Colony-picked human mesenchymal stromal cells (hMSCs, male, age 22) were provided by the Institute of Regenerative Medicine (Temple, Texas).[32] Briefly, mononuclear cells were separated from bone marrow aspirate using density centrifugation. They were plated to achieve adherent hMSCs and harvested when cells reached 60–80% confluence. These cells were called passage zero (P0) cells and were further expanded and harvested as passage one (P1). To achieve sufficient cells for seeding onto scaffolds, P1 cells were expanded in proliferation medium (PM), consisting of α-MEM (Gibco), 10% fetal bovine serum (Lonza), 2 mM L-glutamin (Gibco), 0.2 mM ascorbic acid (Sigma), 100 U/mL penicillin and 100 mg/mL streptomycin (Gibco) and 1 ng/mL recombinant bFGF (Instruchemie). Cells were harvested for further sub-cultures when they become 80-90% confluence. Electrospun scaffolds were placed in cell culture plates and pressed with rubber O-rings (Eriks BB, The Netherlands) to prevent them from floating. The specimens were sterilized by immersion in 70% (v/v) ethanol for 15 min for three times. Subsequently, scaffolds were washed for 1 min with PBS for three times and immersed in BM overnight before cell seeding. A density of 5×10^3 cells/cm^2 was used to seed hMSCs onto electrospun scaffolds. Cell-scaffold constructs were cultured for up to 28 days in BM consisting of PM without bFGF, OM comprising BM supplemented with 1×10^{-6} M dexamethasone), MM composed of OM plus b-glycerol phosphate, and CM containing DMEM (Gibco, Carlsbad, CA) supplemented with 1% ITS premix (Micronic BV), 50 μg/mL ascorbic acid (Sigma), 100 units/mL penicillin (Life technologies), 100 μg/mL streptomycin (Life technologies), 100 nM dexamethasone (Sigma), 40 μg/mL proline (Sigma, St. Louis, MO), 100 μg/mL sodium pyruvate (Life technologies), 0.01 μg/mL TGFβ1 (R&D systems). Culture experiments were performed in an incubator with 5% CO_2 humid atmosphere at 37 °C. Culture medium was refreshed every 2 days.

Metabolic activity. Cell culture medium was removed from cell-scaffold constructs and supplemented with a medium containing 10% (v/v) PrestoBlue™ reagent (Life technologies). The

cell-scaffold constructs were incubated at 37 °C for 1 h in the dark. Fluorescence was measured at 590 nm using a multiabel plate reader (Perkin Elmer Victor3 1420, USA).

Cell morphology analysis: Cell morphology and attachment on scaffolds was determined by SEM using an XL 30 ESEM-FEG (Philips, The Netherlands). Briefly, samples were rinsed twice with PBS, fixed with 10% formalin for 2h. After washing with PBS two times, the samples were dehydrated with a gradient ethanol series, dried by using critical point drying (Balzers CPD 030) and sputtered with gold (Cressington) before SEM analysis.

Quantification of DNA. Samples were washed with PBS three times and stored at -80 °C overnight. After thawing, samples were lysated for 16 h with a Tris/EDTA buffer containing 1mg/mL proteinase K, 185 ug/mL iodoacetamine (Sigma Aldrich) and 10 ug/mL Pepstatin A (Sigma Aldrich). Subsequently, the quantification of the total amount of DNA was examined by using the CyQuant® DNA assay (Molecular Probes, Eugene, USA) as previously reported[33]. Lysate was pipetted in duplicate to a black 96-well plate, followed by addition of NaCl-EDTA buffer containing component B of the kit (20×) and RNase (1000×). The plate was incubated for 1h at room temperature. Subsequently, Gr-dye solution was added and the samples were incubated for 15 min. The fluorescence were determined using a spectrophotometer (Victor3 1420, Perkin Elmer, USA) at an excitation wavelength of 480 nm and emission wavelength of 520 nm.

ALP assay: The protocol of measuring ALP activity was similar to previous study.[34] Briefly, the cell-scaffold constructs were digested for 1 h at room temperature in a cell lysis buffer at a pH 7.8 composed of 0.1 M KH_2OPO_4, 0.1 M K_2HPO_4 and 0.1% Triton X-100. Then, cell lysates were pipetted in duplicate to 96-well plate. After addition of CDP-star® (Roche Life Science), the lysate were incubated for 15 min at room temperature. The measurements were performed on a Victor3 1420 (Perkin Elmer, USA) plate reader. The value of ALP activity was normalized to DNA quantity per scaffold.

GAG assay: Cell-scaffold constructs were washed with PBS three times and stored at -80 °C for at least 24 h. After thawing, the constructs were digested for 16 h with Tris/EDTA buffer as

mentioned above. The amount of GAG was determined spectrophotometrically after reaction with 16 mg of dimethylmethylene blue dye (DMMB, Sigma-Aldrich) in a 10 mM hydrochloric acid solution containing 3.04 g/L of glycine and 2.37 g/L of NaCl. The absorbance was measured on a micro plate reader (Multiskan GO, Thermo Fisher, USA). The amount of GAG was calculated using a standard of chondroitin sulfate (Sigma-Aldrich).

Histological staining: ALP staining was carried out by using an Alkaline phosphatase kit (Sigma-Aldrich). Samples were fixed in 40% citrate working solution in acetone for 30 s and rinsed with deionized water three times. Alkaline dye mixture was added and incubated for 30 min at room temperature in the dark. Samples were finally rinsed thoroughly with deionized water three times. For ARS assay, after fixation in 10% formalin for 1 h, samples were rinsed with PBS three times, washed twice with distilled water and stained with a freshly filtered 2% aqueous Alizarin red solution (pH 4.2) for 2 min. The excess stain was washed off thoroughly with distilled water. To quantify the orange-red coloration of ARS, the protocol was performed as described in a previous study.[35] After removing excess water, samples were transferred to a microcentrifuge tube. A 10% acetic acid solution was added and incubated for 30 min at room temperature with shaking. The slurry was centrifuged for 15 min at 20,000 g after vortexing for 30s. Then, the supernatant was transferred to a new 1.5-mL microcentrifuge tube. A 10% ammonium hydroxide was utilized to neutralize the acid. Aliquots of the supernatant were read in triplicate at 405 nm in 96-well format using opaque-walled, transparent-bottomed plates (Fisher Lifesciences). All the images for ALP staining and ARS staining were taken using a stereomicroscope (Nikon SMZ800 with Q-imaging Retiga 1300 camera).

Quantitative PCR analysis: To analyze the gene expression of hMSCs on scaffolds, total RNA was isolated using a combination of TRIzol with a NucleoSpinRNAII ISOLATON kit (Bioke). Briefly, scaffolds at day 7 and day 28 were rinsed with PBS three times and 1mLof TRIzol was added to each sample. After addition of chloroform, phase separation occurred by centrifugation at 12,000 g. The aqueous phase containing RNA was collected, mixed with equal volume of 75% (v/v)

ethanol and loaded onto an RNA binding column. After a series of purification steps, RNA was re-suspended in RNase-free water and collected using a clean Eppendorf® tubs by centrifugation at 12,000 g. The concentration and purity of RNA were measured by using a spectrophotometer (ND 1000, Nanodrop Technologies, USA). iScript (Bio-Rad, Veenendaal, the Netherlands) was used for the cDNA synthesis following the manufacturer's instruction. Quantitative polymerase chain reaction (qPCR) was carried out using SYBR-green supermix (Bio-Rad). Cycling parameters for running qPCR were set as follows: initial denaturation at 95 °C for 10 min, followed by 40 cycles of 15 s at 95 °C and 1 min at 60 °C. The sequences of the analyzed primers are shown in Table S3. Data are expressed as fold change relative to controls, after normalizing to B_2M.

Statistical analysis: All data points are expressed as mean ± standard deviation. Statistical difference was determined by using two-way analysis of variance (ANOVA), followed by a Tukey's post-hoc test. A value of $p < 0.05$ was considered statistically significant.

Supporting Information

Supporting Information is available from the Wiley Online Library or from the author.

Acknowledgements

H.C. thanks the China Council Scholarship programme for financial support (Grant # 2011614016). FP7 COST Action MP1206 "Electrospun Nano-fibres for bio inspired composite materials and innovative industrial applications" is acknowledged.

Reference

[1] H. Chen, X. Fan, J. Xia, P. Chen, X. Zhou, J. Huang, J. Yu, P. Gu, *Int. J. Nanomedicine*. **2011**, *6*, 453.

[2] S. Agarwal, J. H. Wendorff, A. Greiner, *Polymer*. **2008**, *49*, 5603.

[3] B. D. Ulery, L. S. Nair, C. T. Laurencin, *J. Polym. Sci., Part B: Polym. Phys.* **2011**, *49*, 832.

[4] B. M. Holzapfel, J. C. Reichert, J.-T. Schantz, U. Gbureck, L. Rackwitz, U. Nöth, F. Jakob, M. Rudert, J. Groll, D. W. Hutmacher, *Adv. Drug Del. Rev.* **2013**, *65*, 581.

[5] I. Bechthold, K. Bretz, S. Kabasci, R. Kopitzky, A. Springer, *Chem. Eng. Technol.* **2008**, *31*, 647.

[6] M. Gigli, M. Fabbri, N. Lotti, R. Gamberini, B. Rimini, A. Munari, Eur. Polym. J. Ms. Ref. No.: EUROPOL-D-15-00633 .

[7] M. Soccio, N. Lotti, M. Gigli, L. Finelli, M. Gazzano, A. Munari, *Polym. Int.* **2012**, *61*, 1163.

[8] a) G. C. Reilly, A. J. Engler, *J. Biomech.* **2010**, *43*, 55; b) A. B. Faia-Torres, S. Guimond-Lischer, M. Rottmar, M. Charnley, T. Goren, K. Maniura-Weber, N. D. Spencer, R. L. Reis, M. Textor, N. M. Neves, *Biomaterials*. **2014**, *35*, 9023; c) A. Higuchi, Q.-D. Ling, Y. Chang, S.-T. Hsu, A. Umezawa, *Chem. Rev.* **2013**, *113*, 3297.

[9] M. Gigli, N. Lotti, M. Gazzano, L. Finelli, A. Munari, *J. Appl. Polym. Sci.* **2012**, *126*, 686.

[10] M. Gigli, N. Lotti, M. Gazzano, L. Finelli, A. Munari, Polym. Eng. & Sci. **2013**, *53*, 491.

[11] a) M. Soccio, N. Lotti, M. Gazzano, M. Govoni, E. Giordano, A. Munari, *React. Funct. Polym.* **2012**, *72*, 856; b) C. Gualandi, M. Soccio, M. Govoni, S. Valente, N. Lotti, A. Munari, E. Giordano, G. Pasquinelli, M. L. Focarete, *J. Bioact. Compat. Polym.* **2012**, *27*, 244; c) C. Gualandi, M. Soccio, E. Saino, M. L. Focarete, N. Lotti, A. Munari, L. Moroni, L. Visai, *Soft Matter*. **2012**, *8*, 5466.

[12] a) M. Gigli, M. Govoni, N. Lotti, E. D. Giordano, M. Gazzano, A. Munari, *RSC Adv.* **2014**, *4*, 32965; b) M. Gigli, N. Lotti, M. Vercellino, L. Visai, A. Munari, *Mater. Sci. Eng. C.* **2014**, *34*, 86.

[13] M. Gigli, A. Negroni, G. Zanaroli, N. Lotti, F. Fava, A. Munari, *React. Funct. Polym.* **2013**, *73*, 764.

[14] a) M. Rizvi, P. Kumar, D. Katti, A. Pal, *Acta Biomater.* **2012**, *8*, 4111; b) X. Wei, Z. Xia, S.-C. Wong, A. Baji, *Int. J. Exp. Comput. Biomech.* **2009**, *1*, 45.

[15] M. Gigli, A. Negroni, M. Soccio, G. Zanaroli, N. Lotti, F. Fava, A. Munari, *Green Chem.* **2012**, *14*, 2885.

[16] M. Mochizuki, M. Hirami, *Polym. Adv. Technol.* **1997**, *8*, 203.

[17] A. Mentink, M. Hulsman, N. Groen, R. Licht, K. J. Dechering, J. van der Stok, H. A. Alves, W. J. Dhert, E. P. van Someren, M. J. Reinders, *Biomaterials.* **2013**, *34*, 4592.

[18] A. Nandakumar, L. Yang, P. Habibovic, C. van Blitterswijk, *Langmuir.* **2009**, *26*, 7380.

[19] A. Nandakumar, A. Barradas, J. de Boer, L. Moroni, C. van Blitterswijk, P. Habibovic, *Biomatter.* **2013**, *3*. 23705

[20] W. Liu, J. Lipner, J. Xie, C. N. Manning, S. Thomopoulos, Y. Xia, *ACS Appl. Mater. Interfaces.* **2014**, *6*, 2842.

[21] Y. R. V. Shih, C. N. Chen, S. W. Tsai, Y. J. Wang, O. K. Lee, *Stem Cells.* **2006**, *24*, 2391.

[22] A. C. Bean, R. S. Tuan, *Biomed. Mater.* **2015**, *10*, 015018.

[23] B. C. Heng, T. Cao, E. H. Lee, *Stem Cells.* **2004**, *22*, 1152.

[24] G. S. Stein, J. B. Lian, *Endocr. Rev.* **1993**, *14*, 424.

[25] N. M. Teplyuk, M. Galindo, V. I. Teplyuk, J. Pratap, D. W. Young, D. Lapointe, A. Javed, J. L. Stein, J. B. Lian, G. S. Stein, *J. Biol. Chem.* **2008**, *283*, 27585.

[26] A. Polini, D. Pisignano, M. Parodi, R. Quarto, S. Scaglione, *PLoS One.* **2011**, *6*, e26211.

[27] R. Franceschi, Crit. Rev. Oral Biol. Med. **1999**, *10*, 40.

[28] D. Fayol, G. Frasca, C. Le Visage, F. Gazeau, N. Luciani, C. Wilhelm, *Adv. Mater.* **2013**, *25*, 2611.

[29] H. Akiyama, Modern Rheumatology 2008, 18, 213; S. Q. Liu, Q. Tian, J. L. Hedrick, J. H. P. Hui, P. L. R. Ee, Y. Y. Yang, *Biomaterials.* **2010**, *31*, 7298.

[30] G. Siegel, T. Kluba, U. Hermanutz-Klein, K. Bieback, H. Northoff, R. Schäfer, *BMC Med.* **2013**, *11*, 146.

[31] C. Kiani, C. Liwen, Y. J. WU, J. Y. Albert, B. Y. Burton, *Cell Res.* **2002**, *12*, 19.

[32] C. M. DiGirolamo, D. Stokes, D. Colter, D. G. Phinney, R. Class, D. J. Prockop, *Br. J. Haematol.* **1999,** *107*, 275.

[33] A. Leferink, W. Hendrikson, J. Rouwkema, M. Karperien, v. C. Blitterswijk, L. Moroni, *J. Tissue Eng. Regen. Med.* DOI: 10.1002/term.1842

[34] J. Zhang, X. Luo, D. Barbieri, A. M. Barradas, J. D. de Bruijn, C. A. Van Blitterswijk, H. Yuan, *Acta Biomater.* **2014**, *10*, 3254.

[35] a) C. A. Gregory, W. G. Gunn, A. Peister, D. J. Prockop, *Anal. Biochem.* **2004**, *329*, 77; b) A. K. Gaharwar, S. M. Mihaila, A. Swami, A. Patel, S. Sant, R. L. Reis, A. P. Marques, M. E. Gomes, A. Khademhosseini, *Adv. Mater.* **2013**, *25*, 3329.

Table 1. Polymer and scaffold characterization.

Polymer	M_n[a] (g/mol)	PDI[a]	T_g[b] (°C)	$T_{m,\ BDG}$[b] (°C)	$T_{m,\ BS}$[b] (°C)	$\Delta H_{m,\ BDG}$[b] (J/g)	$\Delta H_{m,\ BS}$[b] (J/g)	WCA[c] (°)
PBS	34600	2.5	-32	/	115	/	75	96 ± 1
PBS/PBTDG	37000	2.6	-45	/	113	/	33	81 ± 2
$P(BS_{10}BTDG_{10})$	30200	2.5	-44	/	100	/	30	79 ± 4
PBS/PBDG	23600	2.8	-29	63	114	28	34	72 ± 2
$P(BS_{11}BDG_{11})$	19700	2.3	-30	/	106	/	35	74 ± 2

[a] by GPC performed on polymers in form of powder; [b] by DSC performed on polymeric scaffolds; [c] by WCA performed on polymers in form of film

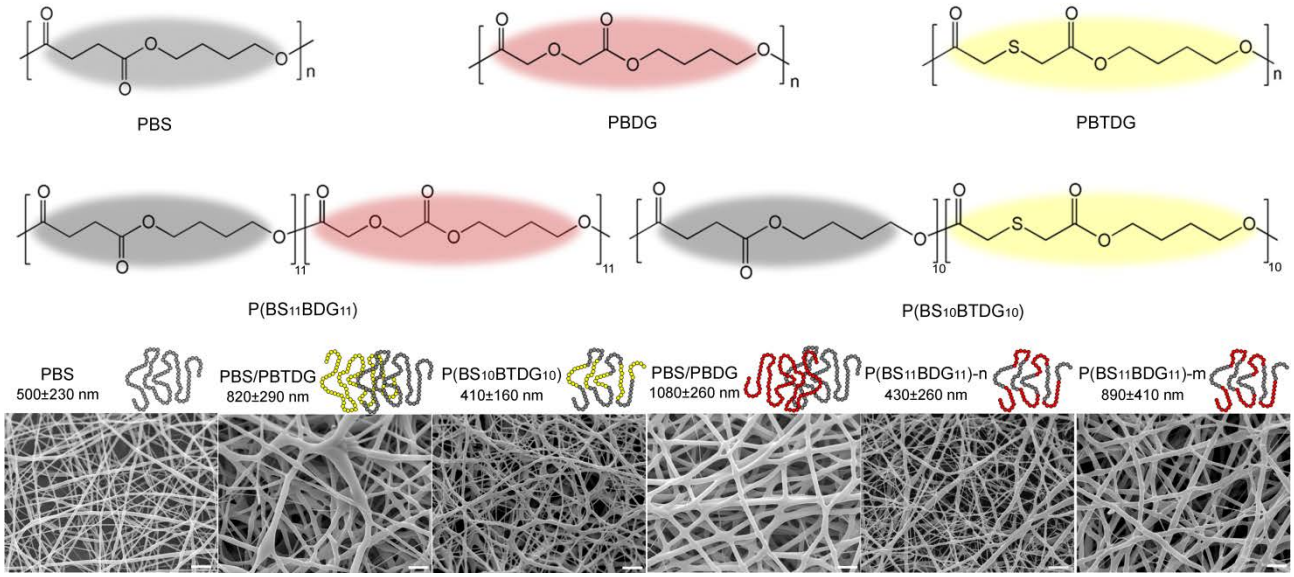

Figure 1. Polymer chemical formulas, SEM micrographs and fibre dimensions of the obtained scaffolds.

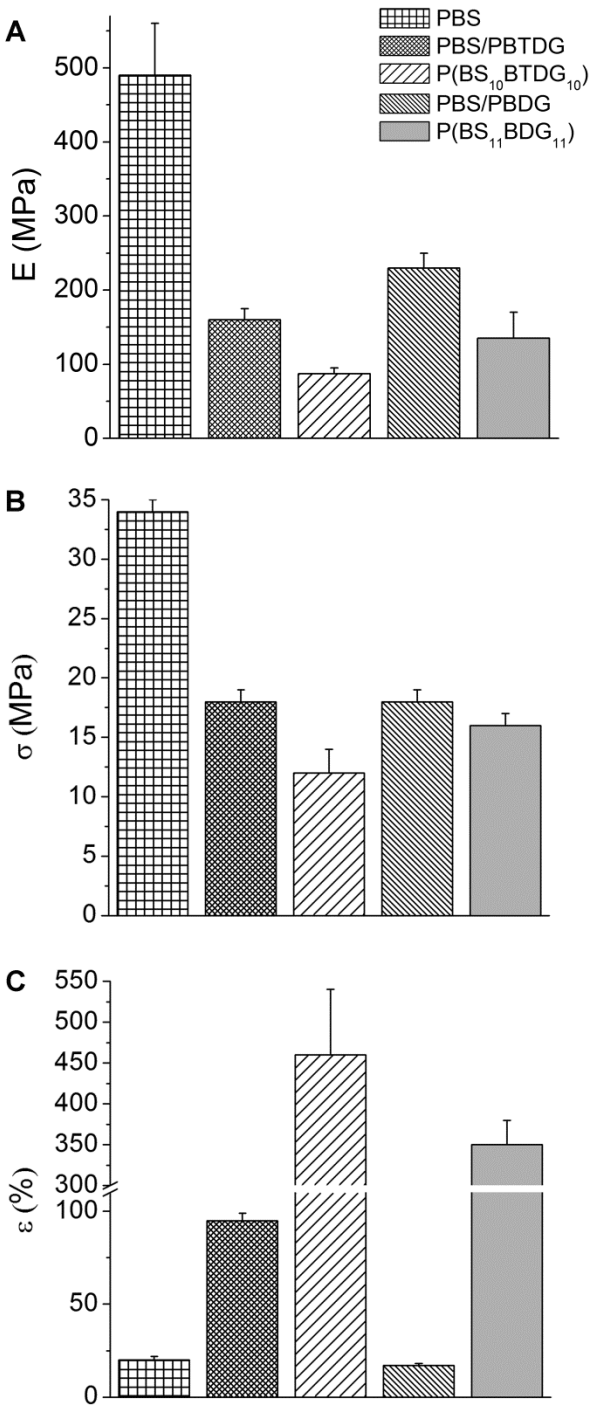

Figure 2. (A) Elastic modulus E; (B) stress at break σ_b and (C) deformation to break ε_b of the polymers under investigation.

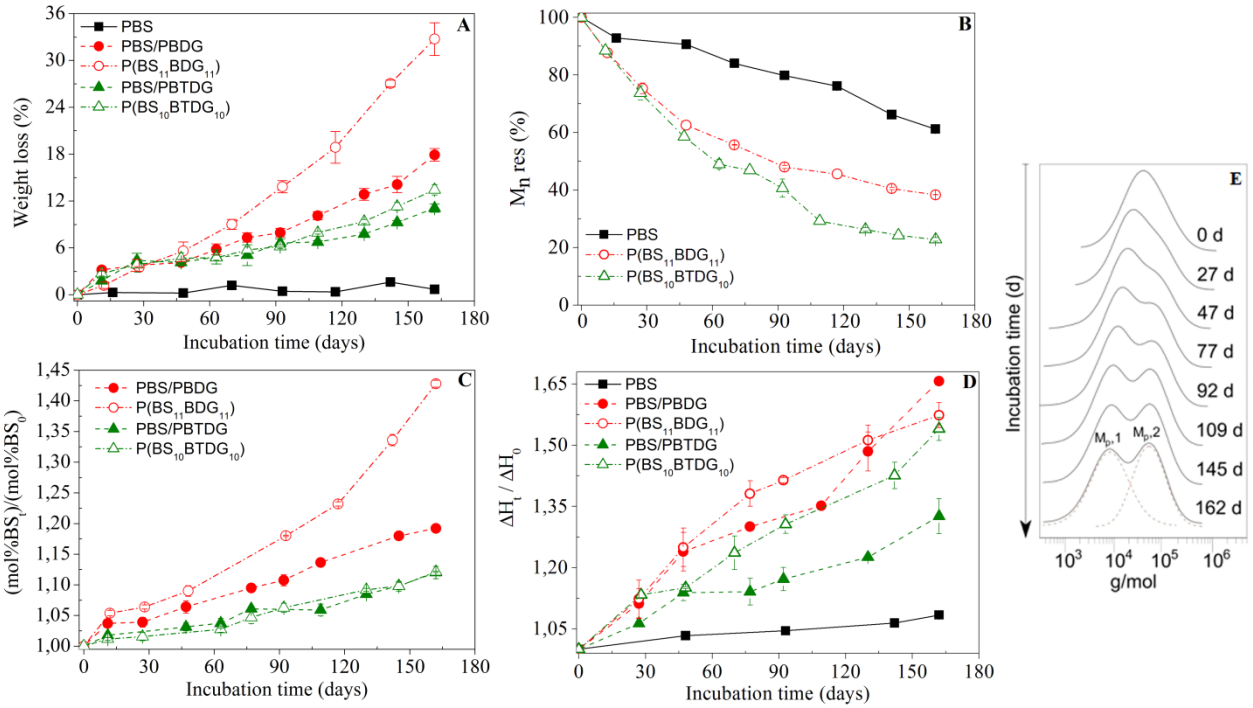

Figure 3. Hydrolytic degradation of polymeric scaffolds under investigation as a function of incubation time. (A) percentage weight loss; (B) percentage residual number molecular weight; (C) increase in BS mol% content; (D) normalized heat of fusion; (E) GPC traces of PBS/PBDG blend as a function of incubation time.

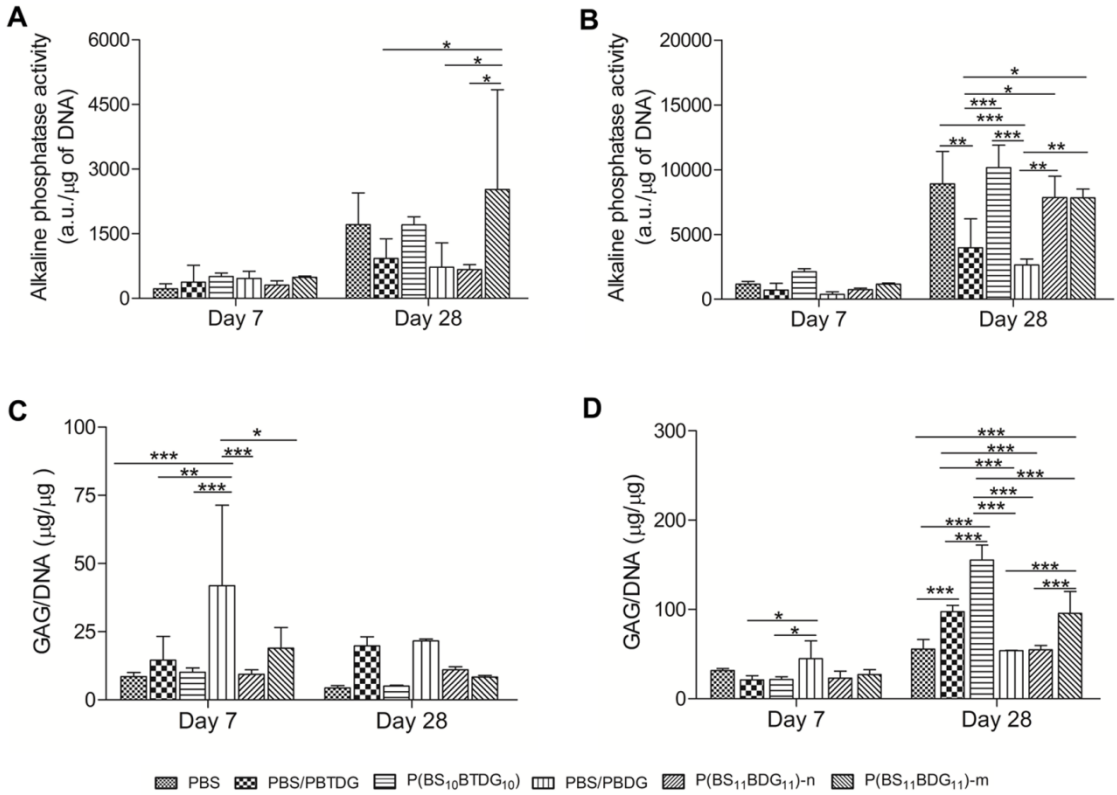

Figure 4. ALP activity of hMSCs cultured on scaffolds in BM (A) and OM (B) at days 7 and 28. The final results of ALP activity level was normalized by DNA amount. GAG production of

hMSCs cultured on scaffolds in BM (C) and CM (D) at day 7 and day 28. *p<0.05, **p < 0.01 , ***p < 0.001.

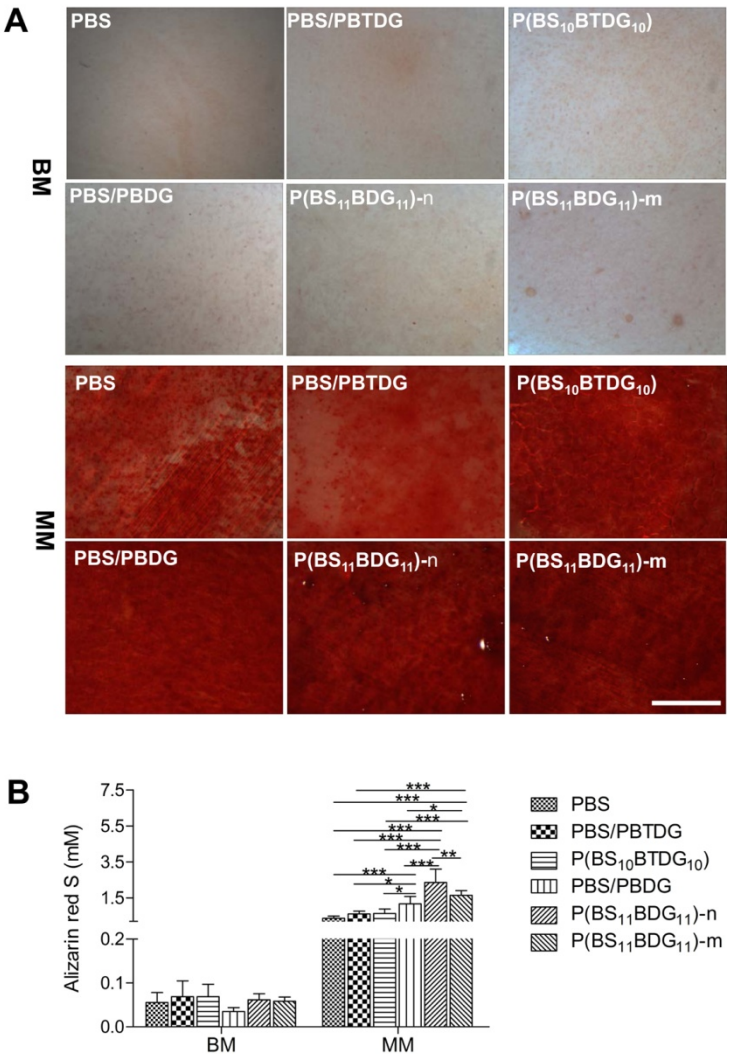

Figure 5. Mineralization of hMSCs on scaffolds was investigated after 28 days of culture in BM and MM. The production of calcium was stained with ARS (A), Scale bar = 1 mm. (B) Quantification of the calcium deposition per scaffold by ARS staining at day 28. *p<0.05

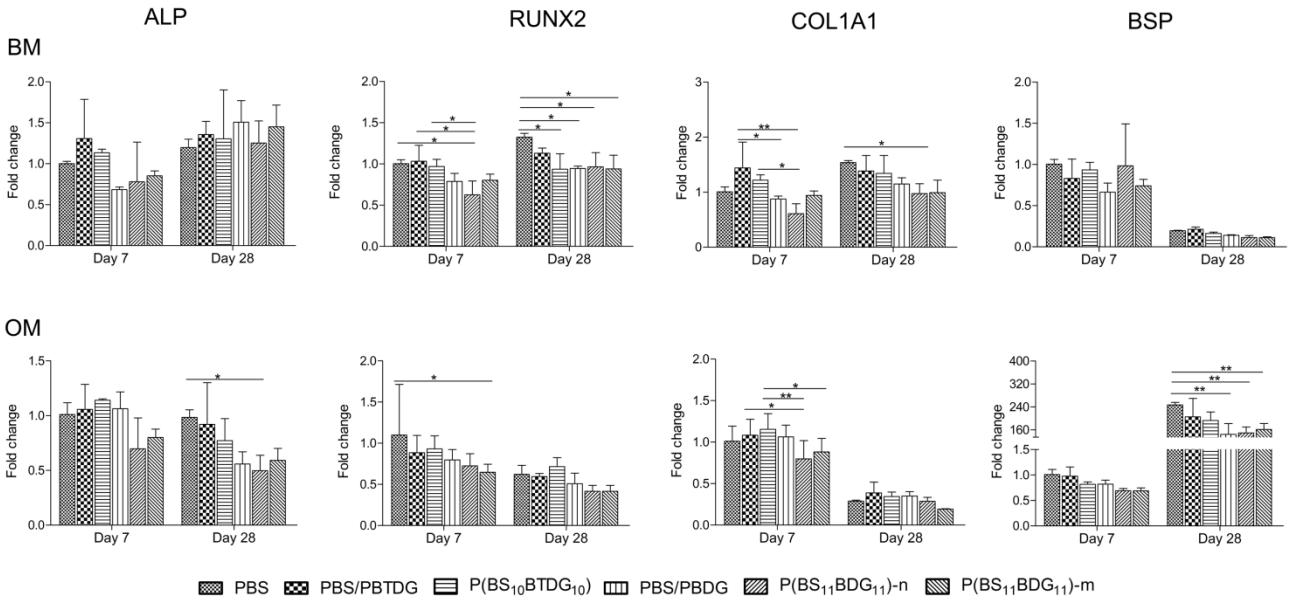

Figure 6. Quantitative RT-PCR gene expression analysis of osteoblast-related genes. Gene expression was normalized for PBS scaffolds of day 7 in both BM and OM. *p<0.05, **p < 0.01.

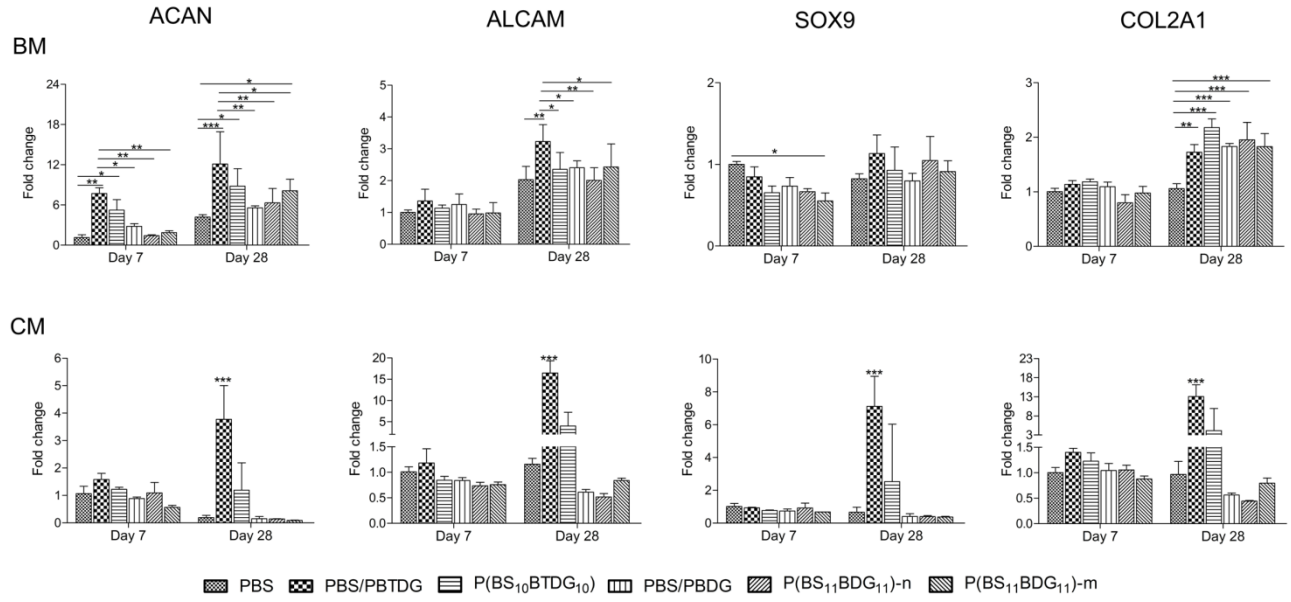

Figure 7. Quantitative RT-PCR gene expression analysis of chondrogenisis-related genes. Gene expression was normalized for day 7 PBS scaffolds in both BM and OM. *p<0.05, **p < 0.01 , ***p < 0.001.

Supporting Information

Tailoring Chemical and Physical Properties of Fibrous Scaffolds from Multiblock Copolyesters Containing Ether and Thio-ether Linkages for Skeletal Differentiation of Human Mesenchymal Stromal Cells

Honglin Chen[§], Matteo Gigli[§], Chiara Gualandi, Roman Truckenmuller, Clemens van Blitterswijk, Nadia Lotti, Andrea Munari, Maria Letizia Focarete, Lorenzo Moroni**

Table S1. Electrospinning operating conditions.

Polymer	solvent mixture (v:v)	conc. (w/v%)	voltage (kV)	flow rate (ml/h)	D[a] (cm)
PBS	DCM:2-CE (80:20)	23	14	0.6	15
PBS/PBDG	HFIP	25	20	0.3	15
$P(BS_{11}BDG_{11})$-m[b]	DCM:2-CE (90:10)	35	17	0.6	20
$P(BS_{11}BDG_{11})$-n[c]	HFIP	25	22	0.5	15
PBS/PBTDG	HFIP	25	19	0.5	15
$P(BS_{10}BTDG_{10})$	HFIP	25	23	0.5	15

[a] D = needle-to-collector distance; [b] "m" indicates micrometric fibers; [c] "n" indicates nanometric fibers.

Table S2. Peak molecular weight as a function of incubation time for PBS/PBDG and PBS/PBTDG.

	PBS/PBDG		PBS/PBTDG	
Incubation time (days)	M_p, 1	M_p, 2	M_p, 1	M_p, 2
0	40600	/	51400	/
27	24700	58800	37900	/
47	18500	58600	32000	59300
77	14200	58600	26100	59400
92	12000	58100	18800	59000
109	10700	56600	12500	57500
145	8200	51100	9700	52100
162	5400	50900	8700	51000

Table S3. Sequences of primers used in real time RT-PCR.

Gene	Forward primer 5' to 3'	Reverse primer 5' to 3'
B2M	ACAAAGTCACATGGTTCACA	GACTTGTCTTTCAGCAAGGA
ALP	ACAAGCACTCCCACTTCATC	TTCAGCTCGTACTGCATGTC
RUNX2	TGGTTACTGTCATGGCGGGTA	TCTCAGATCGTTGAACCTTGCTA
COL1A1	GAGGGCCAAGACGAAGACATC	CAGATCACGTCATCGCACAAC
BSP	CCCCACCTTTTGGGAAAACCA	TCCCCGTTCTCACTTTCATAGAT
COL2A1	CGTCCAGATGACCTTCCTACG	TGAGCAGGGCCTTCTTGAG
SOX9	TGGGCAAGCTCTGGAGACTTC	ATCCGGGTGGTCCTTCTTGTG
ACAN	AGGCAGCGTGATCCTTACC	GGCCTCTCCAGTCTCATTCTC
ALCAM	ACGATGAGGCAGACGAGATAAGT	CAGCAAGGAGGAGACCAACAAC

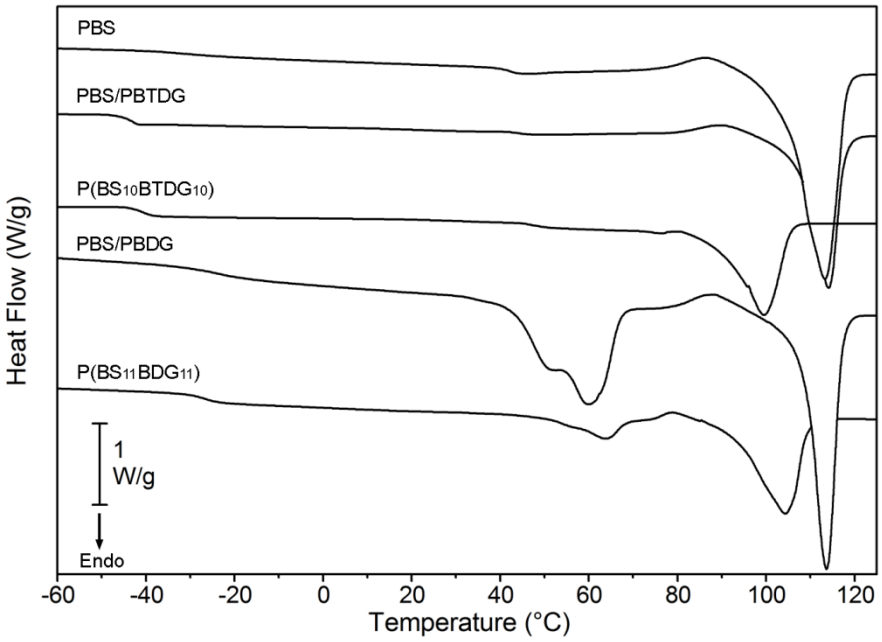

Figure S1. Calorimetric curves of the polymeric scaffolds under investigation.

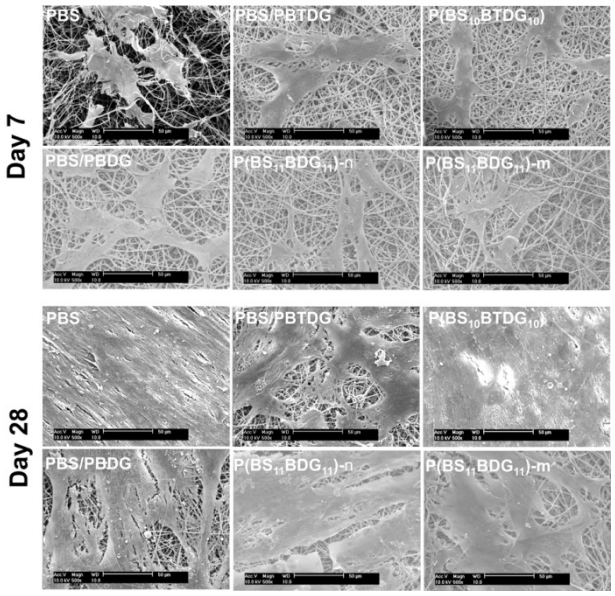

Figure S2. SEM images of hMSCs cultured on scaffolds in BM at day 7 and day 28.

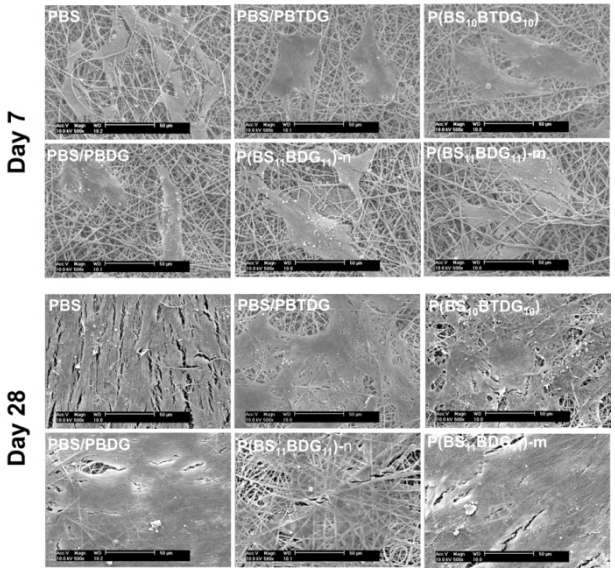

Figure S3. SEM images of hMSCs cultured on scaffolds in OM at day 7 and day 28.

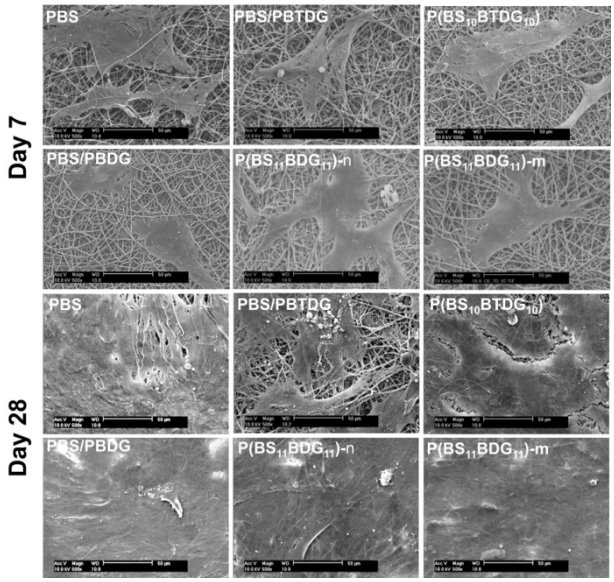

Figure S4. SEM images of hMSCs cultured on scaffolds in CM at day 7 and day 28.

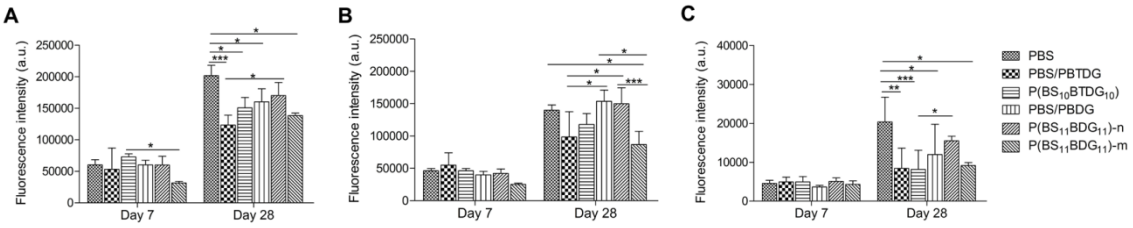

Figure S5. Metabolic activity of hMSCs cultured on scaffolds in BM(A), OM(B) and CM (C) at day 7 and day 28. *p<0.05, **p < 0.01 , ***p < 0.001.

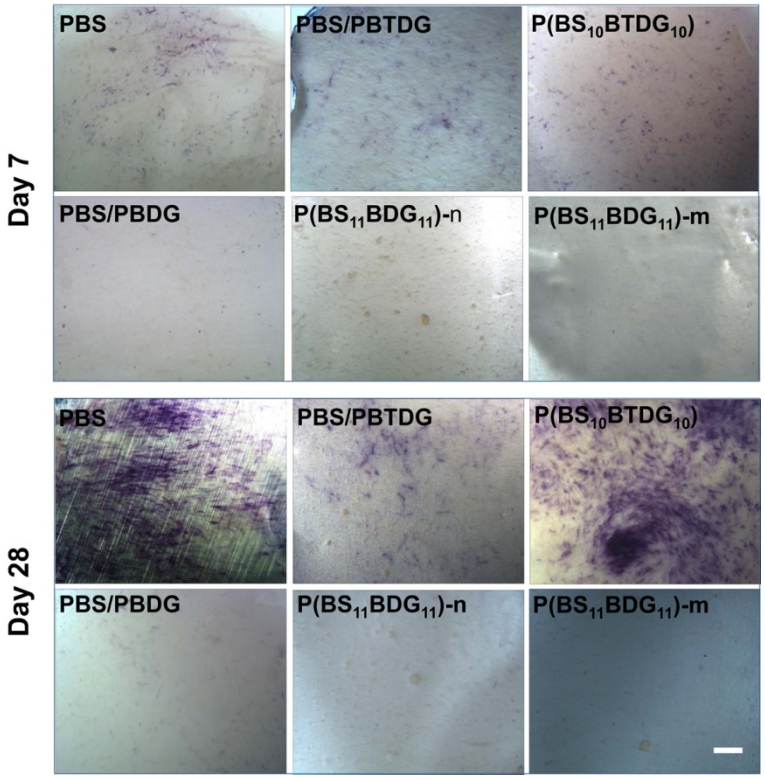

Figure S6. The staining of alkaline phosphatase enzyme activity for hMSCs on scaffolds in BM at day 7 and day 28. Scale bar =1mm.

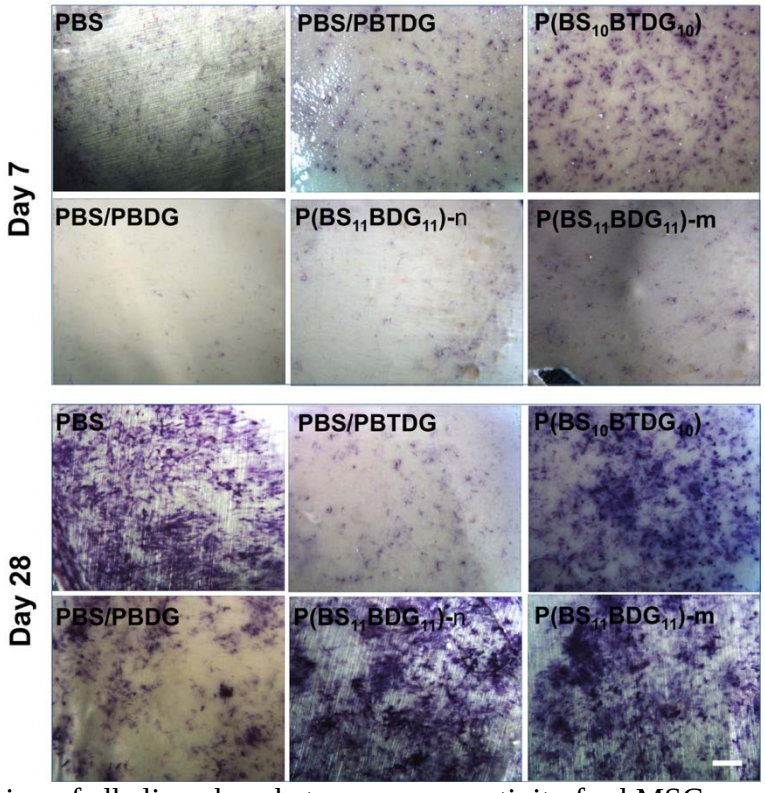

Figure S7. The staining of alkaline phosphatase enzyme activity for hMSCs on scaffolds in OM at day 7 and day 28. Scale bar =1mm.